

DIDO: Deep Inertial Quadrotor Dynamical Odometry

Kunyi Zhang^{1,2}, Chenxing Jiang^{1,2}, Jinghang Li², Sheng Yang³, Teng Ma³, Chao Xu^{1,2} and Fei Gao^{1,2}

Abstract—In this work, we propose an interoceptive-only state estimation system for a quadrotor with deep neural network processing, where the quadrotor dynamics is considered as a perceptive supplement of the inertial kinematics. To improve the precision of multi-sensor fusion, we train cascaded networks on real-world quadrotor flight data to learn IMU kinematic properties, quadrotor dynamic characteristics, and motion states of the quadrotor along with their uncertainty information, respectively. This encoded information empowers us to address the issues of IMU bias stability, dynamic constraints, and multi-sensor calibration during sensor fusion. The above multi-source information is fused into a two-stage Extended Kalman Filter (EKF) framework for better estimation. Experiments have demonstrated the advantages of our proposed work over several conventional and learning-based methods.

I. INTRODUCTION

Aerial robots are popular autonomous vehicles prevalently used in entertainment and industrial applications. To locate themselves, exteroceptive sensors (e.g., LiDAR and cameras) play a prominent role in common scenarios. However, when encountering degenerate cases where features are either heavily repeated or insufficient, these robots in-turn rely on interoceptive sensors (e.g., IMU and rotors) to accumulately deduct their poses. Inaccurate dynamic models, unestimated noise and bias can lead to rapid divergence of state propagation.

Recent approaches [1]–[6], for exteroceptive sensor disabled scenarios, choose to learn the correspondence between IMU sequences and the relative poses through a data-driven approach. Although these works show the potential of deep neural networks for estimation, they are typically designed for scenes of walking pedestrians or low-degree-of-freedom (DOF) ground vehicles, which is difficult to generalize to aerial robots.

As a 4 DOF under-actuated system, the quadrotor can provide strong motion constraints, which are not fully exploited in general state estimation system. The algorithm proposed in [7] can obtain tilt and velocity of a quadrotor using only the tachometer and IMU data. However, its dynamics model only considers a quadratic thrust model and a first-order drag model, which the quadrotors do not strictly conform to. NeuroBEM [8] employs a neural network to compensate

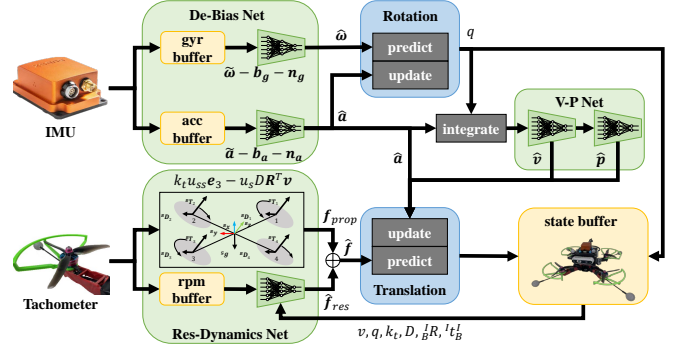


Fig. 1: The filter pipeline of proposed Deep Inertial quadrotor Dynamical Odometry (DIDO). The green parts are cascaded networks designed for learning kinematic properties, quadrotor dynamic characteristics and motion states, the blue parts are EKF process.

for the unmodeled parts such as airflow during the dynamics modeling, but it is not utilized for state estimation.

Therefore, this paper proposes a deep inertial-dynamical odometry framework, employing neural networks to learn both IMU and dynamics properties for better performance in quadrotor state estimation. The kinematic properties of IMU (accelerometer and gyroscope) are learned by two convolutional neural networks (CNN) for measurement de-biasing and de-noising. The dynamic characteristics of quadrotors, with respect to the propeller rotation speed and states, are learned to compensate for mechanistic modeling by a CNN. Besides, the velocity and position of the quadrotor are observed in real-time by a recurrent neural network (RNN). Finally, the networks mentioned above are fused with IMU and tachometer measurements in a two-stage EKF framework. Specifically, in the stage of rotation, the de-biased angular velocity and acceleration are fused to get accurate rotation by gravity-alignment. In the translation stage, the modified dynamics is regard as process model, and the dynamic constraints along with velocity and position from network are considered as observation models, for accurate estimation of kinematic, dynamic states and extrinsic parameters. The contributions of this letter are enumerated below:

- 1) We present a series of networks to learn the IMU kinematics and quadrotor dynamics, demonstrating the capability to provide precise observations with only raw IMU and tachometer data.
- 2) We propose a complete state estimation system that combines quadrotor dynamic constraints and network observations within a two-stage EKF to jointly estimate kinematic, dynamic states and extrinsic parameters.

This work was supported by the National Key Research and Development Program of China (Grant NO. 2020AAA0108104), Alibaba Innovative Research (AIR) Program, and National natural Science Foundation of China under Grant 62003299.

¹State Key Laboratory of Industrial Control Technology, Institute of Cyber-Systems and Control, Zhejiang University, Hangzhou 310027, China.

²Huzhou Institute, Zhejiang University, Huzhou 313000, China.

³Alibaba DAMO Academy Autonomous Driving Lab, Hangzhou 311121, China.

E-mail: {kunyizhang, fgaoaa}@zju.edu.cn

II. RELATED WORKS

A. IMU Learning based estimation

IONet [1], RoNIN [2] and RIDI [3] are designed to estimate the poses of pedestrians. IONet [1] uses a long short-term memory network (LSTM) based network, whose inputs are accelerometer and gyroscope measurements within a time window in the world coordinate system (rotation is provided by the phones' API). RoNIN [2] proposes three different neural network architectures to solve the inertial navigation problem: LSTM, temporal convolutional network (TCN), and residual network (ResNet). These models regress the velocity and displacement of the pedestrian in 2 dimensions. RIDI [3] design a two-stage system, which first classifies the motion of pedestrians into four holding modes by a support vector machine (SVM), and then outputs the accelerometer compensation by four support vector regression machine (SVR) with specific modes. The displacement of a pedestrian is finally obtained after double integration.

AI-IMU [4], IDOL [5], TLIO [6] and CTIN [9] combines deep neural networks with filter framework to obtain better performance. AI-IMU [4] is specially designed for the purpose of vehicle's pose estimation, using a CNN to estimate the covariance of accelerometer and gyroscope measurements and applying them to an invariant extended Kalman filter (IEKF). In addition, the filter considers the vehicle sideslip constraints as well as the motion constraints in the vertical direction. IDOL [5] and TLIO [6] are both applied for pedestrian's pose estimation. IDOL [5] is divided into a rotation estimation module and a translation estimation module. In the rotation module, an LSTM network with gyroscope, accelerometer, and magnetometer data as inputs is trained to output the rotation, which is fused with the rotation obtained by integrating the gyroscope using the extended Kalman filter (EKF). In the position estimation module, the position is regressed using the LSTM network after converting the acceleration to the world coordinate system using the above rotation. TLIO [6] uses a ResNet network similar to RoNIN [2] to estimate pedestrian displacements without yaw, and a stochastic cloning extended Kalman filter (SCEKF) [10] framework to fuse the output values of the network with raw IMU measurements, for estimating position, rotation, and sensor bias in a tightly coupled manner. CTIN [9] uses ResNet and LSTM to obtain the local and global embeddings, and feeds these two embeddings into two multi-headed Transformers [11] to obtain the velocity and its covariance.

B. Quadrotor dynamics and state estimation

A quadrotor is usually powered by four rotating propellers, and the relationship between rotors' speed and dynamical states can be obtained by modeling the quadrotor's mechanics. Traditionally, a simple quadratic model is widely adopted, where the thrust and axial torque generated by the rotor are proportional to the square of their rotation speed with a constant factor [12]. The momentum theorem does not take into account either the motion of the rotor

in air or the rotor-rotor and rotor-body interactions. The blade-element-momentum (BEM) theory [13]–[15] combines blade-element theory and momentum theory to alleviate the difficulty of calculating the induced velocity and accurately capture aerodynamic force and torque acting on single rotor in a wide range of operating conditions. But it also does not take into account any interactions between different propellers and body.

NeuroBEM [8] uses a neural network to fit the residuals between the real quadrotor dynamics and the calculated values from the BEM theory. It [8] takes the rotor speed and kinematic states as network's inputs to allow the quadrotor to perform highly maneuverable trajectories. In [7], the authors estimate the tilt and velocity of the quadrotor in the body frame by applying only the tachometer and gyroscope as inputs and taking the accelerometer as observation. VIMO [16] and VID-Fusion [17] also consider the constraints of quadrotor dynamics in visual inertial fusion to improve the robustness and accuracy of pose estimation.

III. KINEMATIC AND DYNAMIC NETWORK DESIGN

A. Preliminaries

1) *IMU Model*: IMU measurements include the gyroscope $\tilde{\omega}$ and non-gravitational acceleration \tilde{a} , which are measured in the IMU frame (the \mathcal{I} frame) and given by:

$$\begin{aligned}\mathcal{I}\tilde{\omega} &= \mathcal{I}\omega + \mathcal{I}b_{\omega} + n_{\omega}, \\ \mathcal{I}\tilde{a} &= \mathcal{I}a + \mathcal{I}b_a + \frac{\mathcal{G}}{\mathcal{I}}\mathbf{R}^{\top}\mathbf{g} + n_a,\end{aligned}\quad (1)$$

where $\mathcal{I}\omega$ and $\mathcal{I}a$ are the true angular velocity and acceleration, $\mathcal{G}\mathbf{g} = [0, 0, 9.8]$ is the gravity vector in the gravity-aligned frame (the \mathcal{G} frame), $\frac{\mathcal{G}}{\mathcal{I}}\mathbf{R}$ is the rotation matrix from the \mathcal{I} frame to the \mathcal{G} frame, n_{ω} and n_a are the additive Gaussian white noise in gyroscope and acceleration measurements, b_{ω} and b_a are the bias of IMU modeled as random walk:

$$\begin{aligned}n_{\omega} &= \mathcal{N}(0, \sigma_{\omega}^2), & b_{\omega} &= \mathcal{N}(0, \sigma_{b_{\omega}}^2), \\ n_a &= \mathcal{N}(0, \sigma_a^2), & b_a &= \mathcal{N}(0, \sigma_{b_a}^2).\end{aligned}\quad (2)$$

2) *Quadrotor Dynamics*: Because the propagation of kinematic states are driven by multiple propulsion units in a quadrotor system, we model the Newtonian dynamics according to [18]. The total driving force of a quadrotor in the body frame (the \mathcal{B} frame) is the sum of the thrust ${}^{\mathcal{B}}\mathbf{F}_t$ and drag force ${}^{\mathcal{B}}\mathbf{F}_d$ generated by each propulsion unit as follow:

$$\begin{aligned}{}^{\mathcal{B}}\mathbf{F} &= \sum_{i=1}^4 ({}^{\mathcal{B}}\mathbf{F}_{t_i} - {}^{\mathcal{B}}\mathbf{F}_{d_i}) \\ &= \sum_{i=1}^4 (k_t u_i^2 \mathbf{e}_3 - u_i D {}^{\mathcal{B}}\mathbf{v}_i),\end{aligned}\quad (3)$$

where k_t is the thrust coefficient for the propellers, $D = \text{diag}(d_x, d_y, d_z)$ is the matrix of effective linear drag coefficients, $\mathbf{e}_3 = [0, 0, 1]^{\top}$ is the z axis in any frame, and u_i and ${}^{\mathcal{B}}\mathbf{v}_i$ are the rotation speed and velocity of the i -th rotor, respectively. Actually, the velocity of each rotor is:

$${}^{\mathcal{B}}\mathbf{v}_i = {}^{\mathcal{B}}\mathbf{v} + {}^{\mathcal{B}}\omega \times {}^{\mathcal{B}}\mathbf{r}_i^{\mathcal{B}}, \quad (4)$$

where ${}^B\mathbf{v}$ and ${}^B\boldsymbol{\omega}$ are the linear and angular velocity of the quadrotor's center of mass (CoM), ${}^B\mathbf{r}_i^B$ is the position of the i -th rotor relative to the CoM . To simplify the calculation, we ignore the velocity discrepancy of different rotors and express it as:

$${}^B\mathbf{v}_i \approx {}^B\mathbf{v}. \quad (5)$$

The input notations are abbreviated as:

$$U_{ss} = \sum_{i=1}^4 u_i^2, \quad U_s = \sum_{i=1}^4 u_i, \quad (6)$$

so we can obtain the Newtonian equation in the \mathcal{G} frame:

$$m \frac{d}{dt} ({}^G\mathbf{v}) = {}^G\mathbf{R} (k_t U_{ss} \mathbf{e}_3 - U_s D_B^G \mathbf{R}^{\top G} \mathbf{v}_B^G) - m^G \mathbf{g}. \quad (7)$$

B. Network Design

1) *De-Bias Net*: As an interoceptive sensor, IMU often requires several integrations to obtain the kinematic states, but the system would drift or diverge because of the failure to accurately estimate the accelerometer bias ${}^I\hat{\mathbf{b}}_a$ and gyroscope bias ${}^I\hat{\mathbf{b}}_\omega$. So, we design a *De-Bias Net* to learn IMU's kinematic characteristics while de-biasing and de-noising. The two *De-Bias Nets* for accelerometer and gyroscope have the same network architecture, a 1D version of ResNet [19] with only one residual block to boost the inference process. And, fully-connected layers are extended to output.

The respective input features of both *De-Bias Nets* are historical raw accelerometer measurements ${}^I\tilde{\mathbf{a}}$ and gyroscope measurements ${}^I\tilde{\boldsymbol{\omega}}$, each output is ${}^I\hat{\mathbf{b}}_a$ and ${}^I\hat{\mathbf{b}}_\omega$ at every moment, separately.

We individually define two Mean Square Error (MSE) loss functions $\mathcal{L}_{MSE,a}$ and $\mathcal{L}_{MSE,g}$ for accelerometer and gyroscope on the following integrated increments:

$$\begin{aligned} \mathcal{L}_{MSE,a} &= \frac{1}{N} \sum_{i=1}^N \|\mathbf{v}_{i,i+n} - \hat{\mathbf{v}}_{i,i+n}\|_2^2, \\ \mathcal{L}_{MSE,g} &= \frac{1}{N} \sum_{i=1}^N \|\log((\hat{\mathbf{q}}_{i,i+n})^* \otimes \mathbf{q}_{i,i+n})\|_2^2. \end{aligned} \quad (8)$$

Specially,

$$\begin{aligned} \hat{\mathbf{v}}_{i,i+n} &= \int_i^{i+n} {}^G\mathbf{R}({}^I\tilde{\mathbf{a}} - {}^I\hat{\mathbf{b}}_a) dt, \\ \mathbf{v}_{i,i+n} &= {}^G\mathbf{v}_{i+n} - {}^G\mathbf{v}_i, \\ \hat{\mathbf{q}}_{i,i+n} &= {}^I_{i+n} \hat{\mathbf{q}} = \int_i^{i+n} \frac{1}{2} {}^I_{i+n} \mathbf{q} \otimes ({}^I_t \tilde{\boldsymbol{\omega}} + {}^I_t \hat{\mathbf{b}}_\omega) dt, \\ \mathbf{q}_{i,i+n} &= {}^I_{i+n} \mathbf{q} = ({}^G_{i+n} \mathbf{q})^* \otimes {}^G_{i+n} \mathbf{q}, \end{aligned} \quad (9)$$

where, $\mathbf{v}_{i,i+n}$ and $\mathbf{q}_{i,i+n}$ are the ground truth velocity increment and relative rotation of each sliding window, n is the window size and N is the batch size, \otimes means the quaternion multiplication. In training, ${}^G_{\mathcal{I}}\mathbf{R}$ is the ground truth rotation.

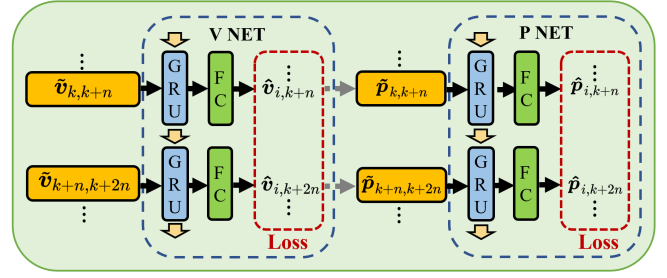


Fig. 2: The network structure for V-P Net

2) *Res-Dynamics Net*: DActually, the dynamic model of quadratic thrust and approximately linear drag in Eq. (3) can not accurately model quadrotors because of complicated effects related to airflow and so on. Therefore, like NeuroBEM [8], we adopt the same ResNet [19] as *De-Bias Nets* to capture the unmodeled part of the quadrotor dynamics.

We regard a sliding window of angular and linear velocity in the \mathcal{B} and rotor speed data as input features to train the *Res-Dynamics Net* in a supervised fashion, whose history window size is set to 20.

In order to fit the compensation force and fuse it into the EKF framework reasonably, a MSE loss function is replaced by a Negative log-likelihood (NLL) loss [20] after the former loss stabilizes and converges:

$$\begin{aligned} \mathcal{L}_{MSE,f} &= \frac{1}{N} \sum_{i=1}^N \|{}^B\mathbf{a}_{\mathcal{B}i}^G - {}^B\hat{\mathbf{a}}_{\mathcal{B}i}^G\|_2^2, \\ \mathcal{L}_{NLL,f} &= \frac{1}{2N} \sum_{i=1}^N \log \det(\hat{\boldsymbol{\Sigma}}_{\mathbf{a}_i}) + \frac{1}{2} \mathcal{L}_{MSE,f}. \end{aligned} \quad (10)$$

Specially,

$$\begin{aligned} {}^B\hat{\mathbf{a}}_{\mathcal{B}}^G &= \frac{1}{m} \left(k_t U_{ss} \mathbf{e}_3 - U_s D_B^G \mathbf{R}^{\top G} \mathbf{v}_{\mathcal{B}}^G + \hat{\mathbf{f}}_{res} \right) - {}^G\mathbf{R}^{\top G} \mathbf{g}, \\ {}^B\mathbf{a}_{\mathcal{B}}^G &= {}^G\mathbf{R}^{\top G} \mathbf{a}_{\mathcal{I}}^G + {}^B\boldsymbol{\omega} \times ({}^B\boldsymbol{\omega} \times {}^B\mathbf{t}_{\mathcal{B}}^{\mathcal{I}}) + {}^B\boldsymbol{\alpha} \times {}^B\mathbf{t}_{\mathcal{B}}^{\mathcal{I}}, \end{aligned} \quad (11)$$

where, $\hat{\mathbf{f}}_{res}$ is the output of *Res-Dynamics Net*, ${}^G\mathbf{a}_{\mathcal{I}}^G$ is the true acceleration fitted by ground truth, $\{\boldsymbol{\omega}, \boldsymbol{\alpha}, \mathbf{t}_{\mathcal{B}}^{\mathcal{I}}\}$ in the \mathcal{B} frame are converted from the \mathcal{I} frame by ${}^B_{\mathcal{I}}\mathbf{R}$.

3) *V-P-Net*: Even though *De-Bias Nets* help to reduce the bias of IMU measurements, the remaining tiny offset of acceleration would not avoid the cumulative error in the integration process. Therefore, we design a cascaded GRU network to learn velocity and position approximation that has less error accumulation over a long period of time. As every dimension of velocity and position are independent to each other, we adopt three cascaded GRU networks for the X , Y and Z axes separately. The cascaded architecture has two parts: *V-Net* and *P-Net*, these two parts have the same structure as shown in Fig. 2.

We firstly integrate the de-biased acceleration as follow:

$$\tilde{\mathbf{v}}_{k,k+m} = \int_k^{k+m} {}^G_{\mathcal{I}}\mathbf{R}({}^I_t \tilde{\mathbf{a}} - {}^I_t \hat{\mathbf{b}}_a) dt, \quad (12)$$

where the size of an integration window is m without overlap among each window.

Each element of $\hat{\mathbf{v}}_{k,k+m}$ and integration time dt are input features of *V-Net*. The hidden state is passed to fully-connected layers to regress the uniaxial velocity relative to the start of a sequence.

Then, we use results of the *V-Net* to calculate the displacement over the integration window as shown in Eq. (13), which is the input feature of *P-Net* to regress the uniaxial position relative to the start of a sequence.

$$\tilde{\mathbf{p}}_{k,k+m} = \hat{\mathbf{v}}_{k,k+m} \mathbf{t}_{k,k+m} - \frac{1}{2} \int_k^{k+m} \frac{g}{\mathcal{I}_t} \mathbf{R}(\mathcal{I}_t \tilde{\mathbf{a}} - \mathcal{I}_t \hat{\mathbf{b}}_a) dt^2, \quad (13)$$

where

$$\hat{\mathbf{v}}_{k+m} = \hat{\mathbf{v}}_{i,k+m} + \hat{\mathbf{v}}_i, \quad (14)$$

$\hat{\mathbf{v}}_i$ is the initial velocity of the sequence, $\hat{\mathbf{v}}_{i,k+m}$ is the result of the *V-Net* in the $(k+m)$ -th step and $\mathbf{t}_{k,k+m}$ is the duration of the integration window.

Similarly, we use MSE and NLL loss over the whole sequence as follows:

$$\begin{aligned} \mathcal{L}_{\text{MSE},v,p} &= \frac{1}{NM} \sum_{i=0}^N \sum_{j=0}^M (\|\mathbf{v}_{i,j} - \hat{\mathbf{v}}_{i,j}\|_2^2 + \|\mathbf{p}_{i,j} - \hat{\mathbf{p}}_{i,j}\|_2^2), \\ \mathcal{L}_{\text{NLL},v,p} &= \frac{1}{2NM} \sum_{i=1}^N \sum_{j=0}^M (\log \det(\hat{\Sigma}_{\mathbf{v}_{i,j}}) + \log \det(\hat{\Sigma}_{\mathbf{p}_{i,j}})) \\ &\quad + \frac{1}{2} \mathcal{L}_{\text{MSE},v,p}. \end{aligned} \quad (15)$$

Specially,

$$\mathbf{v}_{i,j} = {}^G \mathbf{v}_{\mathcal{I}_j}^G - {}^G \mathbf{v}_{\mathcal{I}_i}^G, \quad (16)$$

where, M is the sequence length, N is batch size, $\hat{\mathbf{v}}_{i,j}$ and $\hat{\mathbf{p}}_{i,j}$ are the j -th predicted uniaxial velocity and position relative to the start of sequence i , $\mathbf{v}_{i,j}$ and $\mathbf{p}_{i,j}$ are the ground truth, $\hat{\Sigma}_{\mathbf{v}_{i,j}}$ and $\hat{\Sigma}_{\mathbf{p}_{i,j}}$ are the covariance of uniaxial velocity and position.

C. Dataset Preparation

There are only the Blackbird dataset [21] and the VID dataset [22] in the flying robot community that contain quadrotor dynamics. The former trajectories are too repetitive to generalize well for networks, while the latter suffers from insufficient data for training. Therefore, to satisfy the training requirements, we equip a new quadrotor as a data acquisition platform and record adequate data. The quadrotor assembles 4 tachometers and an additional IMU¹ as shown in Fig. 3, and the ground truth is provided by a VICON² system.

To ensure the diversity of trajectories, we record a total of 274 yaw-constant and yaw-forward trajectories, which include 247 Random, 15 Circle and 12 Figure-8 trajectories. Where Random trajectories are sampled and optimized [23] to be executed by the quadrotor as a smooth trajectory.

To provide high-frequency and accurate supervised data for network training, we first fit the full state of kinematics at the IMU frequency with B-splines [24] in the gravity-aligned

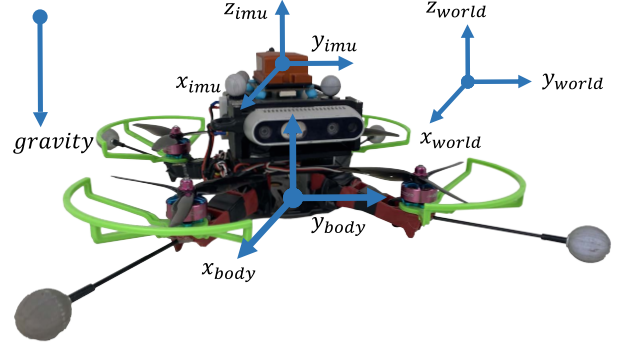


Fig. 3: The quadrotor platform, which assembles an IMU and 4 tachometers, is built for data acquisition.

coordinate frame, and then identify the dynamics model of the quadrotor by offline optimization.

D. Training Details

1) *Covariance Training*: Except for *De-Bias Net*, the mean and covariance outputs of the corresponding networks are available for the remaining three networks. Every covariance $\hat{\Sigma}$ is a 3×3 matrix with 6 degrees of freedom, but a diagonal form is assumed in this paper, and parameterized by 3 coefficients written as:

$$\hat{\Sigma}_{\xi} = \text{diag}(e^{2\hat{\xi}_x}, e^{2\hat{\xi}_y}, e^{2\hat{\xi}_z}). \quad (17)$$

Since it is difficult to converge the direct training covariance by \mathcal{L}_{NLL} , we use \mathcal{L}_{MSE} in the first 20 epoch and then replace by \mathcal{L}_{NLL} .

2) *V-P Net*: When training *V-P Net*, we use different lengths of sequences for training. In experiment, the hidden sizes of GRU are [2, 64, 128, 256], integration window size m is 20.

3) *Data Separation and Optimizer*: We select 200 Random trajectories for training and the remaining as the validation and test sets. Adam optimizer is chose to minimize the loss function, and the initial learning rate is set to 0.0001.

IV. INERTIAL DYNAMICAL FUSION PIPELINE

A. Rotation Stage

In order to avoid the negative feedback of *V-P Net* observations on the rotation, we separate the rotation and translation estimation in a two-stage EKF framework.

1) *State*: In the first rotation stage, there is only the rotation of the \mathcal{I} in the \mathcal{G} frame taken as filter's state:

$$\mathbf{x} = \frac{g}{\mathcal{I}} \mathbf{q}. \quad (18)$$

2) *Process Model*: The rotational equation is given:

$$\begin{aligned} \dot{\mathbf{x}} &= \frac{1}{2} \frac{g}{\mathcal{I}} \mathbf{q} \otimes \mathcal{I} \boldsymbol{\omega} \\ &= \frac{1}{2} \frac{g}{\mathcal{I}} \mathbf{q} \otimes (\mathcal{I} \hat{\boldsymbol{\omega}} + \mathbf{n}_{n_g}), \end{aligned} \quad (19)$$

where $\mathcal{I} \hat{\boldsymbol{\omega}}$ and \mathbf{n}_{n_g} are the gyroscope *De-Bias Net* outputs and their noises.

¹<https://www.xsens.com/mti-300>

²<https://www.vicon.com/>

3) *Measurement Model*: The attitude controllers of most flying robots rely on the complementary filters [25, 26] to obtain attitude observations. Similarly, we consider the gravity alignment condition to obtain the tilt observation:

$$\mathcal{I}\tilde{\mathbf{a}} \approx \mathcal{G}\mathbf{R}^\top \mathcal{G} \mathbf{g} + \mathbf{n}_a. \quad (20)$$

B. Translation Stage

1) *State*: The state of the second stage is defined as:

$$\mathbf{x} = (\mathcal{G}\mathbf{p}_B^\mathcal{G}, \mathcal{G}\mathbf{v}_B^\mathcal{G}, k_t, \mathbf{d}, \mathcal{I}_B\mathbf{q}, \mathcal{I}_B\mathbf{t}_B^\mathcal{I}), \quad (21)$$

where $\mathcal{G}\mathbf{p}_B^\mathcal{G}$ and $\mathcal{G}\mathbf{v}_B^\mathcal{G}$ are respectively the velocity and position of the quadrotor body \mathcal{B} frame expressed in the \mathcal{G} frame, \mathbf{d} is the drag vector of (d_x, d_y, d_z) , and $(\mathcal{I}_B\mathbf{q}, \mathcal{I}_B\mathbf{t}_B^\mathcal{I})$ is the extrinsic parameter between the \mathcal{B} and the \mathcal{I} frame.

2) *Process Model*: We regard the quadrotor dynamics as the input, and express the complete process model as follows:

$$\begin{aligned} \mathcal{G}\dot{\mathbf{p}}_B^\mathcal{G} &= \mathcal{G}\mathbf{v}_B^\mathcal{G}, \\ \mathcal{G}\dot{\mathbf{v}}_B^\mathcal{G} &= \frac{1}{m}\mathcal{G}\mathbf{R}(k_t U_{ss} \mathbf{e}_3 - U_s D_B^\mathcal{G} \mathbf{R}^\top \mathcal{G}\mathbf{v}_B^\mathcal{G} + \mathbf{f}_{res}) - \mathcal{G}\mathbf{g}, \\ \dot{k}_t &= 0, \\ \dot{\mathbf{d}} &= \mathbf{0}, \\ \mathcal{I}_B\dot{\mathbf{q}} &= \mathbf{0}, \\ \mathcal{I}_B\dot{\mathbf{t}}_B^\mathcal{I} &= \mathbf{0}, \end{aligned} \quad (22)$$

where $\mathcal{G}\mathbf{R} = \mathcal{G}\mathbf{R}_B^\mathcal{I}\mathbf{R}$ is the rotation from the quadrotor body \mathcal{B} frame to the \mathcal{G} frame.

3) *Measurement Model*: Firstly, since accelerometer measurements are not used before, we take the inconsistency of the \mathcal{I} and \mathcal{B} frame into account and express the dynamics measurement equation as follow:

$$\begin{aligned} \mathcal{I}\tilde{\mathbf{a}} &= \frac{1}{m}\mathcal{I}_B\mathbf{R}(k_t U_{ss} \mathbf{e}_3 - U_s D_B^\mathcal{G} \mathbf{R}^\top \mathcal{G}\mathbf{v}_B^\mathcal{G} + \mathbf{f}_{res}) \\ &+ \mathcal{I}\boldsymbol{\omega} \times (\mathcal{I}\boldsymbol{\omega} \times \mathcal{I}_B\mathbf{t}_B^\mathcal{I}) + \mathcal{I}\boldsymbol{\alpha} \times \mathcal{I}_B\mathbf{t}_B^\mathcal{I} + \mathbf{n}_a. \end{aligned} \quad (23)$$

What's more, our aforementioned *V-P Net* can be used as observers of velocity and displacement:

$$\begin{aligned} \mathcal{G}\tilde{\mathbf{v}}_B^\mathcal{G} &= \mathcal{G}\mathbf{v}_B^\mathcal{G} - \mathcal{G}\boldsymbol{\omega} \times \mathcal{G}\mathbf{t}_B^\mathcal{I} + \mathbf{n}_{n_v}, \\ \mathcal{G}\tilde{\mathbf{p}}_B^\mathcal{G} &= \mathcal{G}\mathbf{p}_B^\mathcal{G} - \mathcal{G}\mathbf{t}_B^\mathcal{I} + \mathbf{n}_{n_p}, \end{aligned} \quad (24)$$

where $\boldsymbol{\omega}, \mathbf{t}_B^\mathcal{I}$ in the \mathcal{G} frame of Eq. (23) and (24) are converted from the \mathcal{I} frame by $\mathcal{I}_B\mathbf{R} = \mathcal{G}\mathbf{R}_B^\mathcal{I}\mathbf{R}^\top$, and $\mathcal{I}\boldsymbol{\alpha} = \frac{d}{dt}\mathcal{I}\boldsymbol{\omega}$. In practice, we low-pass filter the $\boldsymbol{\omega}, \boldsymbol{\alpha}$ to reduce noise.

C. Discrete Extended Kalman Filter

The complete EKF procedures for both rotation and translation can be written in a discretized form as follows:

$$\begin{aligned} \mathbf{x}_{k+1|k} &= \mathbf{A}_k \mathbf{x}_{k|k} + \mathbf{B}_k \mathbf{u}_k, \\ \mathbf{P}_{k+1|k} &= \mathbf{A}_k \mathbf{P}_{k|k} \mathbf{A}_k^\top + \mathbf{B}_k \mathbf{W} \mathbf{B}_k^\top, \\ \mathbf{K}_{k+1} &= \mathbf{P}_{k+1|k} \mathbf{H}^\top (\mathbf{H} \mathbf{P}_{k+1|k} \mathbf{H}^\top + \mathbf{R})^{-1}, \\ \mathbf{x}_{k+1|k+1} &= \mathbf{x}_{k+1|k} \oplus (\mathbf{K}_{k+1} (\mathbf{z} - h(\mathbf{x}_{k+1|k}))), \\ \mathbf{P}_{k+1|k+1} &= (\mathbf{I} - \mathbf{K}_{k+1} \mathbf{H}) \mathbf{P}_{k+1|k}, \end{aligned} \quad (25)$$

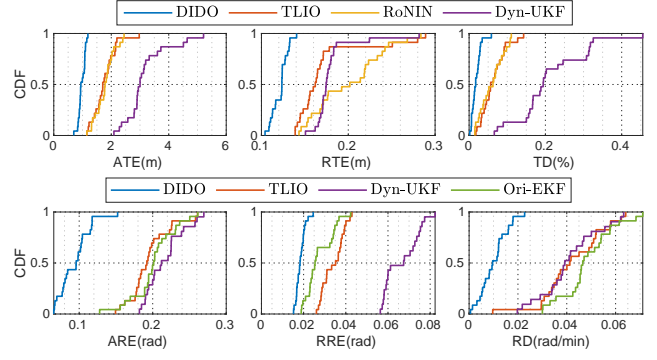


Fig. 4: Plots on the first row are positional comparisons among DIDO, TLIO [6], RoNIN-ResNet [2] and Dyn-UKF [7], while on the second row are rotational comparisons among DIDO, TLIO [6], Dyn-UKF [7] and Ori-EKF [27]. Both error metrics are with respect to the ground truth, and each plot shows the cumulative density function of the chosen metric on the entire test set. The steeper the plots, the better the performance.

where, the Jacobian matrices for EKF are shown in Appendix II and I. Specially, the input and observation covariances for the translation stage are the aforementioned network outputs $\hat{\Sigma}_a$, $\hat{\Sigma}_v$ and $\hat{\Sigma}_p$, respectively.

V. EXPERIMENTS

A. Metrics Definition

In order to assess the performance of our system, we define the metrics including the Absolute Translation Error (ATE, m), the Absolute Rotation Error (ARE, rad), the Relative Translation Error (RTE, m), the Relative Rotation Error (RRE, rad), and the Translation Drift (TD, %), the Rotation Drift (RD, rad/min) as follows:

- $\text{ATE} := \sqrt{\frac{1}{l} \sum_{i=1}^l \|\mathcal{G}\mathbf{p}_i - \mathcal{G}\hat{\mathbf{p}}_i\|_2^2},$
- $\text{ARE} := \sqrt{\frac{1}{l} \sum_{i=1}^l \|\mathcal{G}\hat{\mathbf{q}}_i \ominus \mathcal{G}\mathbf{q}_i\|_2^2},$
- $\text{RTE} := \sqrt{\frac{1}{l} \sum_{i=1}^l \|(\mathcal{G}\mathbf{p}_{i+\Delta t} - \mathcal{G}\mathbf{p}_i) - (\mathcal{G}\hat{\mathbf{p}}_{i+\Delta t} - \mathcal{G}\hat{\mathbf{p}}_i)\|_2^2},$
- $\text{RRE} := \sqrt{\frac{1}{l} \sum_{i=1}^l \|(\mathcal{G}\hat{\mathbf{q}}_i \ominus \mathcal{G}\mathbf{q}_{i+\Delta t}) \ominus (\mathcal{G}\hat{\mathbf{q}}_i \ominus \mathcal{G}\mathbf{q}_i)\|_2^2},$
- $\text{TD} := \|\mathcal{G}\mathbf{p}_l - \mathcal{G}\hat{\mathbf{p}}_l\|_2^2 / (\text{trajectory-length}),$
- $\text{RD} := \|\log(\mathcal{G}\hat{\mathbf{q}}_l \ominus \mathcal{G}\mathbf{q}_l)\|_2^2 / (\text{sequence-duration}),$

where \ominus means the inverse operator of the quaternion multiply \otimes , l is the length of each dataset.

B. Comparison

To better demonstrate our system, we select several conventional and learning-based algorithms to compare the estimation accuracy of 6D pose in the test set.

The proposed DIDO and TLIO [6] are the complete systems, whose results are the filter output. We train and test the former RoNIN-ResNet [2] by providing the ground truth

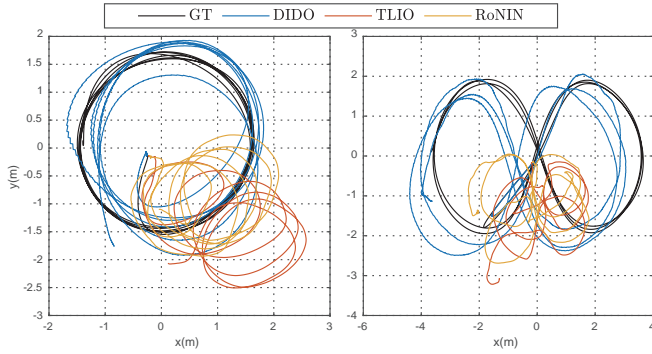


Fig. 5: Top view diagrams of several methods on unseen Circle and Figure-8 trajectories.

rotation, so there is no rotation error shown. There are two conventional algorithms, Dyn-UKF [7] and Ori-EKF [27]. Dyn-UKF [7], integrates the dynamics as a forward process and updates the tilt and velocity in \mathcal{B} frame by the raw accelerometer measurements, while all states are converted to the \mathcal{G} frame by estimated rotation. Ori-EKF [27] only obtains the rotation using the raw accelerometer and gyroscope measurements.

Fig. 4 shows the error distributions among the entire test set, which distinctly shows the proposed DIDO outperforms other methods. Dyn-UKF [7] based only on the momentum theory does not work well, while DIDO compensates for the biased dynamics model resulting in a better performance. Fig. 6 depicts the performance of different methods for each axis. TLIO [6] and RoNIN-ResNet [2] both have unavoidable cumulative drift, while attributing to the *V-P Net*, DIDO has stable position estimation. Besides, *De-Bias Net* decelerates the severe yaw drift, which effectively helps the position estimation. Fig. 5 presents three learning-based methods for position estimation on unseen simple trajectories.

VI. DISCUSSIONS

A. Dynamics or IMU based

In this sensor fusion system, there are two ways to obtain acceleration, one is the accelerometer measurements, and the other is the quadrotor dynamics. Using six degrees of freedom IMU kinematics as a process model cannot fully exploit the constraints of quadrotor aircraft dynamics. Instead, taking quadrotor aircraft dynamics to propagate and the accelerometer measurement to update can help to constrain its tilt and velocity. As a consequence, dynamics-based methods may be superior to IMU-based one in quadrotor estimation system.

B. One-stage or Two-stage

In the proposed method, we separate the rotation and translation processes, which indicates that the latter does not affect the rotation when updating with acceleration, velocity and position. Thus, the advantage of two-stage is that the inconsistency of the network outputs do not influence the rotation directly and thus further affecting the integration of velocity and position. As a counter-example shown in

Fig. 6, the rotation estimation of Dyn-UKF [7] is prone to be impacted by updating of accelerometer measurements. Therefore, we select a two-stage EKF framework in this work.

C. Covariance

Covariances are of great importance in both filter-based and optimization-based frameworks, which are taken as tunable parameters in state estimation system. We train the networks to output the corresponding covariances for better compatibility with the EKF pipeline.

In fact, these covariances from networks may not be the most appropriate parameters for estimation. One possible reason is that we only consider the diagonal elements of the covariance matrix, assuming each axis is independent. And, the covariances only indicate the dispersion of the network output, but are not the weight in the fusion framework. Therefore, in this work, we multiply the network covariances with different adjustable parameters for better fusion.

VII. CONCLUSIONS AND FUTURE WORK

A. Conclusions

In this work, we propose an inertial and quadrotor dynamical odometry system introducing deep neural networks in a two-stage tightly-coupled EKF framework. To the best of our knowledge, this is the first estimation framework that combines IMU, quadrotor dynamics and deep learning methods to simultaneously estimate kinematic and dynamic states, as well as extrinsic parameters. To take full advantage of the two interoceptive sensors, we design deep neural networks to regress the bias of the IMU, the dynamics compensation, motion states of the quadrotor as well as their covariances.

Experimental results have demonstrated that the proposed method outperforms the other conventional and learning-based methods in pose estimation. It is accurate and invulnerable to consider *De-Bias Net* and gravity alignment constraints for rotation estimation. And, it is efficient and versatile to take into account the constraints of both quadrotor dynamics and the deep neural networks for translation estimation. The code and data will be open-sourced to the community ³.

B. Future work

Even though the proposed method makes use of deep neural networks to improve the accuracy of estimation, it still does not guarantee a perfect globally consistent yaw angle and position under long and highly maneuverable flight. The plausible solution is to provide an absolute observation, such as GPS or magnetic compass. Alternatively, some of the proposed modules can be supplied in GPS-free environments with exteroceptive sensors to improve the robustness of estimation.

³<https://zhangkunyi.github.io/DIDO/>

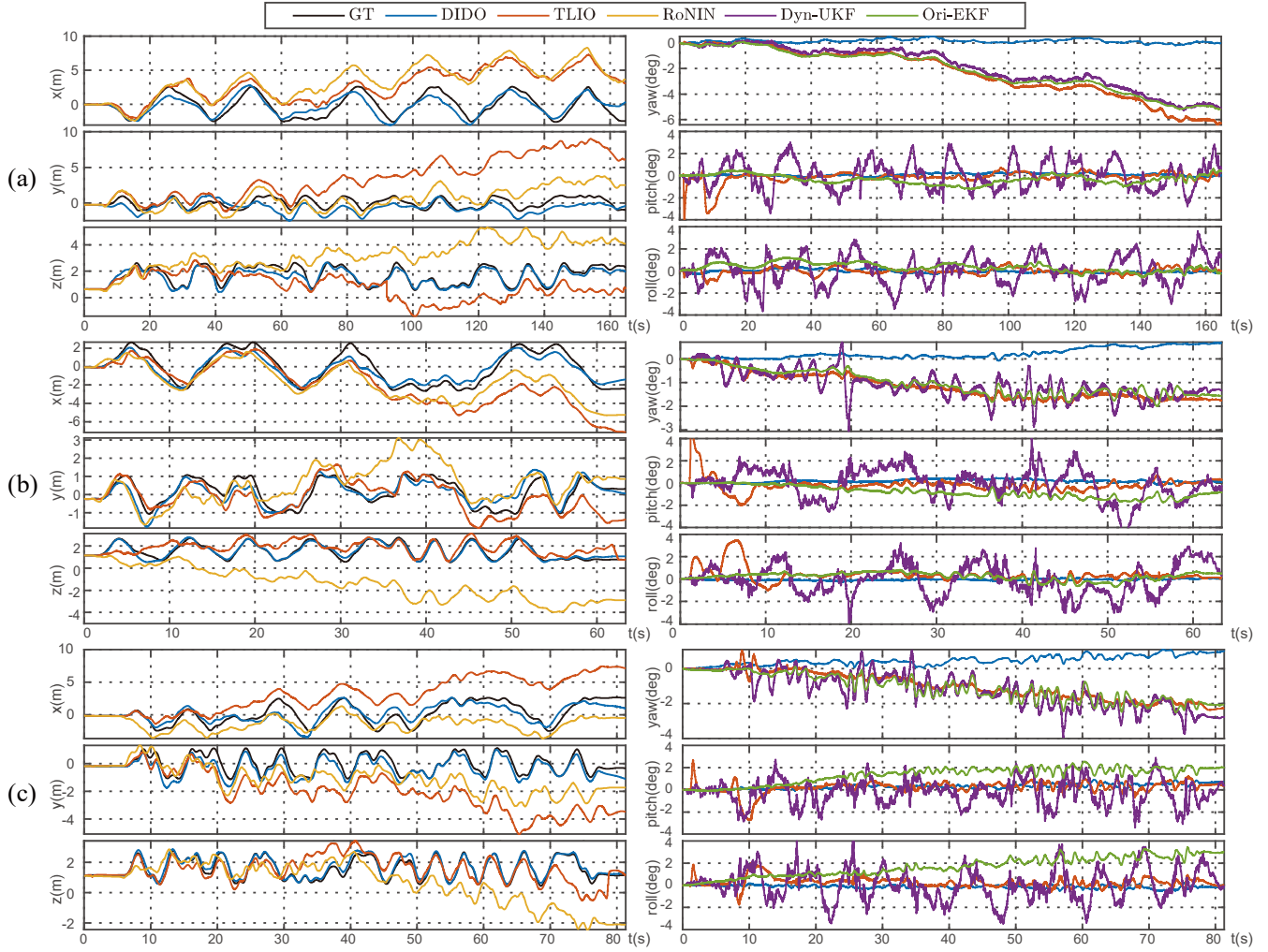


Fig. 6: Demonstration of different methods for position and rotation estimation. We show three Random trajectories corresponding to different max uniaxial velocity (a:0.5m/s, b:1.5m/s, c:2.5m/s) in the test set. For better presentation, the ground truth positions are plotted as black lines in the first column, while ignoring the Dyn-UKF [7] due to its divergence. And the rotation errors are drawn in the second column in the form of Euler angles, which are obtained by making a difference between the estimated rotations and the ground truth.

REFERENCES

- [1] C. Chen, X. Lu, A. Markham, and N. Trigoni, "IONet: Learning to cure the curse of drift in inertial odometry," in *Proceedings of the AAAI Conference on Artificial Intelligence*, vol. 32, no. 1, 2018.
- [2] S. Herath, H. Yan, and Y. Furukawa, "RoNIN: Robust neural inertial navigation in the wild: Benchmark, evaluations, & new methods," in *2020 IEEE International Conference on Robotics and Automation (ICRA)*. IEEE, 2020, pp. 3146–3152.
- [3] H. Yan, Q. Shan, and Y. Furukawa, "RIDI: Robust IMU double integration," in *ECCV*, 2018.
- [4] M. Brossard, A. Barrau, and S. Bonnabel, "AI-IMU dead-reckoning," *IEEE Transactions on Intelligent Vehicles*, vol. 5, no. 4, pp. 585–595, 2020.
- [5] S. Sun, D. Melamed, and K. Kitani, "IDOL: Inertial deep orientation-estimation and localization," *arXiv preprint arXiv:2102.04024*, 2021.
- [6] W. Liu, D. Caruso, E. Ilg, J. Dong, A. I. Mourikis, K. Daniilidis, V. Kumar, and J. Engel, "TLIO: Tight learned inertial odometry," *IEEE Robotics and Automation Letters*, vol. 5, no. 4, pp. 5653–5660, 2020.
- [7] J. Svacha, G. Loianno, and V. Kumar, "Inertial yaw-independent velocity and attitude estimation for high-speed quadrotor flight," *IEEE Robotics and Automation Letters*, vol. 4, no. 2, pp. 1109–1116, 2019.
- [8] L. Bauersfeld, E. Kaufmann, P. Foehn, S. Sun, and D. Scaramuzza, "NeuroBEM: Hybrid aerodynamic quadrotor model," *arXiv preprint arXiv:2106.08015*, 2021.
- [9] B. Rao, E. Kazemi, Y. Ding, D. M. Shila, F. M. Tucker, and L. Wang, "CTIN: Robust contextual transformer network for inertial navigation," *arXiv preprint arXiv:2112.02143*, 2021.
- [10] S. I. Roumeliotis and J. W. Burdick, "Stochastic cloning: A generalized framework for processing relative state measurements," in *Proceedings 2002 IEEE International Conference on Robotics and Automation (Cat. No. 02CH37292)*, vol. 2. IEEE, 2002, pp. 1788–1795.
- [11] A. Vaswani, N. Shazeer, N. Parmar, J. Uszkoreit, L. Jones, A. N. Gomez, Ł. Kaiser, and I. Polosukhin, "Attention is all you need," *Advances in neural information processing systems*, vol. 30, 2017.
- [12] R. Mahony, V. Kumar, and P. Corke, "Multirotor aerial vehicles: Modeling, estimation, and control of quadrotor," *IEEE Robotics and Automation magazine*, vol. 19, no. 3, pp. 20–32, 2012.
- [13] W. Khan and M. Nahon, "Toward an accurate physics-based uav thruster model," *IEEE/ASME Transactions on Mechatronics*, vol. 18, no. 4, pp. 1269–1279, 2013.
- [14] R. Gill and R. D'Andrea, "Propeller thrust and drag in forward flight," in *2017 IEEE Conference on Control Technology and Applications (CCTA)*. IEEE, 2017, pp. 73–79.
- [15] R. Gill and R. D'Andrea, "Computationally efficient force and moment models for propellers in uav forward flight applications," *Drones*, vol. 3, no. 4, p. 77, 2019.
- [16] B. Nisar, P. Foehn, D. Falanga, and D. Scaramuzza, "VIMO: Simultaneous visual inertial model-based odometry and force estimation," *IEEE Robotics and Automation Letters*, vol. 4, no. 3, pp. 2785–2792, 2019.

2019.

- [17] Z. Ding, T. Yang, K. Zhang, C. Xu, and F. Gao, "VID-Fusion: Robust visual-inertial-dynamics odometry for accurate external force estimation," in *2021 IEEE International Conference on Robotics and Automation (ICRA)*. IEEE, 2021, pp. 14 469–14 475.
- [18] J. Svacha, J. Paulos, G. Loianno, and V. Kumar, "Imu-based inertia estimation for a quadrotor using newton-euler dynamics," *IEEE Robotics and Automation Letters*, vol. 5, no. 3, pp. 3861–3867, 2020.
- [19] K. He, X. Zhang, S. Ren, and J. Sun, "Deep residual learning for image recognition," in *CVPR*, 2016.
- [20] D. Chen, N. Wang, R. Xu, W. Xie, H. Bao, and G. Zhang, "RNIN-VIO: Robust neural inertial navigation aided visual-inertial odometry in challenging scenes," in *2021 IEEE International Symposium on Mixed and Augmented Reality (ISMAR)*. IEEE, 2021, pp. 275–283.
- [21] A. Antonini, W. Guerra, V. Murali, T. Sayre-McCord, and S. Karaman, "The blackbird UAV dataset," *The International Journal of Robotics Research*, p. 0278364920908331, 2020.
- [22] K. Zhang, T. Yang, Z. Ding, C. Xu, and F. Gao, "The visual-inertial-dynamical multirotor dataset," *arXiv preprint arXiv:2103.11152*, 2021.
- [23] D. Mellinger and V. Kumar, "Minimum snap trajectory generation and control for quadrotors," in *2011 IEEE international conference on robotics and automation*. IEEE, 2011, pp. 2520–2525.
- [24] P. Geneva and G. Huang, "vicon2gt: Derivations and analysis," University of Delaware, Tech. Rep. RPNG-2020-VICON2GT, 2020, available: <http://udel.edu/~ghuang/papers/tr.vicon2gt.pdf>.
- [25] R. Mahony, T. Hamel, and J.-M. Pfimlin, "Nonlinear complementary filters on the special orthogonal group," *IEEE Transactions on automatic control*, vol. 53, no. 5, pp. 1203–1218, 2008.
- [26] S. O. Madgwick, A. J. Harrison, and R. Vaidyanathan, "Estimation of imu and marg orientation using a gradient descent algorithm," in *2011 IEEE international conference on rehabilitation robotics*. IEEE, 2011, pp. 1–7.
- [27] S. Sabatelli, M. Galgani, L. Fanucci, and A. Rocchi, "A double-stage kalman filter for orientation tracking with an integrated processor in 9-d imu," *IEEE Transactions on Instrumentation and Measurement*, vol. 62, no. 3, pp. 590–598, 2012.

APPENDIX I TRANSLATION STAGE

A. The Jacobian matrix of state-to-state

$$\mathbf{A} = \begin{bmatrix} \mathbf{I}_3 & \mathbf{I}_3\Delta t & \mathbf{0}_{31} & \mathbf{0}_3 & \mathbf{0}_3 & \mathbf{0}_3 \\ \mathbf{0}_3 & \mathbf{f}_{vv} & \mathbf{f}_{vk} & \mathbf{f}_{vd} & \mathbf{f}_{vr} & \mathbf{0}_3 \\ \mathbf{0}_{13} & \mathbf{0}_{13} & 1 & \mathbf{0}_{13} & \mathbf{0}_{13} & \mathbf{0}_{13} \\ \mathbf{0}_3 & \mathbf{0}_3 & \mathbf{0}_{31} & \mathbf{I}_3 & \mathbf{0}_3 & \mathbf{0}_3 \\ \mathbf{0}_3 & \mathbf{0}_3 & \mathbf{0}_{31} & \mathbf{0}_3 & \mathbf{I}_3 & \mathbf{0}_3 \\ \mathbf{0}_3 & \mathbf{0}_3 & \mathbf{0}_{31} & \mathbf{0}_3 & \mathbf{0}_3 & \mathbf{I}_3 \end{bmatrix}, \quad (26)$$

where

$$\begin{aligned} \mathbf{f}_{vv} &= \mathbf{I} - \frac{U_s\Delta t}{m} \mathcal{G}_B \mathbf{R} D \mathcal{G}_B^\top, \\ \mathbf{f}_{vk} &= \frac{U_{ss}\Delta t}{m} \mathcal{G}_B \mathbf{r}_3, \\ \mathbf{f}_{vd} &= \begin{bmatrix} -\frac{\Delta t}{m} (\mathcal{G}_B \mathbf{r}_1 \mathcal{G}_B^\top \mathbf{v}_B^\mathcal{G})^\top \\ -\frac{\Delta t}{m} (\mathcal{G}_B \mathbf{r}_2 \mathcal{G}_B^\top \mathbf{v}_B^\mathcal{G})^\top \\ -\frac{\Delta t}{m} (\mathcal{G}_B \mathbf{r}_3 \mathcal{G}_B^\top \mathbf{v}_B^\mathcal{G})^\top \end{bmatrix}^\top, \\ \mathbf{f}_{vr} &= \frac{k_t U_{ss} \Delta t}{m} \mathcal{G}_B \mathbf{R} [\mathbf{e}_3]_\times \\ &\quad + \frac{U_s \Delta t}{m} \mathcal{G}_B \mathbf{R} [D \mathcal{G}_B^\top \mathbf{v}_B^\mathcal{G}]_\times \\ &\quad - \frac{U_s \Delta t}{m} \mathcal{G}_B \mathbf{R} D [\mathcal{G}_B^\top \mathbf{v}_B^\mathcal{G}]_\times, \end{aligned} \quad (27)$$

and $\mathbf{r}_i = \mathbf{R} \mathbf{e}_i$.

B. The Jacobian matrix of state-to-input

$$\mathbf{B} = [\mathbf{0}_3 \quad \frac{1}{m} \mathcal{G}_B \mathbf{R} \quad \mathbf{0}_{31} \quad \mathbf{0}_3 \quad \mathbf{0}_3 \quad \mathbf{0}_3]^\top. \quad (28)$$

C. The Jacobian matrix of acceleration observation-to-state

$$\mathbf{H}_a = [\mathbf{0}_3 \quad \mathbf{h}_{av} \quad \mathbf{h}_{ak} \quad \mathbf{h}_{ad} \quad \mathbf{h}_{ar} \quad \mathbf{h}_{at}], \quad (29)$$

where

$$\begin{aligned} \mathbf{h}_{av} &= \frac{1}{m} \mathcal{I}_B \mathbf{R} U_s D \mathcal{G}_B^\top, \\ \mathbf{h}_{ak} &= \frac{U_{ss}}{m} \mathcal{I}_B \mathbf{R} \mathbf{e}_3, \\ \mathbf{h}_{ad} &= \begin{bmatrix} -\frac{U_s}{m} (\mathcal{I}_B \mathbf{r}_1 \mathcal{G}_B^\top \mathbf{v}_B^\mathcal{G})^\top \\ -\frac{U_s}{m} (\mathcal{I}_B \mathbf{r}_2 \mathcal{G}_B^\top \mathbf{v}_B^\mathcal{G})^\top \\ -\frac{U_s}{m} (\mathcal{I}_B \mathbf{r}_3 \mathcal{G}_B^\top \mathbf{v}_B^\mathcal{G})^\top \end{bmatrix}^\top, \\ \mathbf{h}_{ar} &= \frac{1}{m} \mathcal{I}_B \mathbf{R} [k_t U_{ss} \mathbf{e}_3 - U_s D \mathcal{G}_B^\top \mathbf{v}_B^\mathcal{G} + \mathbf{f}_{res}]_\times, \\ \mathbf{h}_{at} &= [\mathcal{I}_\omega]_\times [\mathcal{I}_\omega]_\times + [\mathcal{I}_\alpha]_\times. \end{aligned} \quad (30)$$

D. The Jacobian matrix of velocity observation-to-state

$$\mathbf{H}_v = [\mathbf{0}_3 \quad \mathbf{I}_3 \quad \mathbf{0}_{31} \quad \mathbf{0}_3 \quad \mathbf{0}_3 \quad \mathbf{h}_{vt}], \quad (31)$$

where

$$\mathbf{h}_{vt} = \mathcal{I}_B \mathbf{R} [\mathcal{I}_\omega \times \mathcal{I}_B^\top]_\times. \quad (32)$$

E. The Jacobian matrix of position observation-to-state

$$\mathbf{H}_p = [\mathbf{I}_3 \quad \mathbf{0}_3 \quad \mathbf{0}_{31} \quad \mathbf{0}_3 \quad \mathbf{0}_3 \quad \mathbf{h}_{pt}], \quad (33)$$

where

$$\mathbf{h}_{pt} = \mathcal{I}_B \mathbf{R} [\mathcal{I}_B^\top]_\times. \quad (34)$$

APPENDIX II ROTATION STAGE

A. The Jacobian matrix of state-to-state

$$\mathbf{A} = \mathbf{I}_4 + \frac{\Delta t}{2} \begin{bmatrix} 0 & -\mathcal{I}_\omega^\top \\ \mathcal{I}_\omega & [\mathcal{I}_\omega]_\times \end{bmatrix}. \quad (35)$$

B. The Jacobian matrix of state-to-input

$$\begin{aligned} \mathbf{A} &= \frac{\Delta t}{2} \begin{bmatrix} -q_x & -q_y & -q_z \\ q_w & -q_z & q_y \\ q_z & q_w & -q_x \\ -q_y & q_x & q_w \end{bmatrix} \\ &= \frac{\Delta t}{2} \begin{bmatrix} -\mathbf{q}_v \\ q_w \mathbf{I}_3 + [\mathbf{q}_v]_\times \end{bmatrix}, \end{aligned} \quad (36)$$

where $\mathbf{q} = [q_w, q_x, q_y, q_z]^\top = [q_w, \mathbf{q}_v^\top]^\top$.

C. The Jacobian matrix of acceleration observation-to-state

$$\mathbf{A} = 2 [\mathbf{u}_g \quad [\mathbf{u}_g + q_w \mathbf{e}_3]_\times + (\mathbf{q}_v \cdot \mathbf{e}_3) \mathbf{I}_3 - \mathbf{e}_3 \mathbf{q}_v^\top], \quad (37)$$

where $\mathbf{u}_g = \mathbf{e}_3 \times \mathbf{q}_v$.